Scanning Microscopy

Volume 1 | Number 1 Article 1

11-6-1986

A Proposal for a High Resolution Scanning Ion Microprobe Based on Laser Non-Resonant Post-Ionization of Sputtered Atoms

Y. L. Wang
University of Chicago

R. Levi-Setti
University of Chicago

J. Chabala
University of Chicago

Scanning Microscopy, Vol. 1, No. 1, 1987 (Pages 1-11)
Scanning Microscopy International, Chicago (AMF O'Hare), IL 60666 USA

0891-7035/87$3.00+.00

A PROPOSAL FOR A HIGH RESOLUTION SCANNING ION MICROPROBE BASED ON LASER NON-RESONANT POST-IONIZATION OF SPUTTERED ATOMS

Y.L. Wang, R. Levi-Setti* and J. Chabala

Enrico Fermi Institute and Department of Physics
University of Chicago, Chicago, Illinois 60637

(Received for publication July 10, 1986, and in revised form November 06, 1986)

Abstract

A new high resolution scanning ion microprobe (SIM) is described which combines laser non-resonant multiphoton ionization (MPI) and time of flight (ToF) spectroscopy. The proposed instrument is designed to overcome limitations of the conventional secondary ion mass spectrometry (SIMS) method. A pulsed ion probe (with current 1 - 100 pA) is extracted from a liquid metal ion source (LMIS). This beam is purified by a Wien filter, focused to a spot (15 - 150 nm), and scanned across a sample in a raster pattern (512 x 512 pixels). A high power (200 mJ, 193 nm, 500 Hz) ArF pulsed laser – an off-axis ellipsoidal reflector is planned to boost its power density – intercepts the sputtered neutrals, ionizing a large fraction for detection. The resultant ions are collected by a spherical sector energy analyzer and mass resolved by either a reflectron or Poschenrieder type ToF spectrometer. The laser pulse defines the time base for the spectrometer; mass resolution of more than 3000 is feasible. Detailed calculations of the neutrals' sputtering and photoionization yields are given. In particular, an analytical expression for two-photon ionization of sputtered atoms, which optimizes the photon–neutrals overlap, is derived and results plotted. This technique, post-ionization of sputtered atoms (PISA), is shown to permit several high statistical accuracy, high mass and lateral resolution images to be obtained simultaneously, even for elements with high ionization potential or low electron affinity, elements difficult to examine with SIMS. Compared to SIMS, PISA greatly reduces the range of the variation in detected signal as a function of atomic number, facilitating quantification.

Keywords: Scanning ion microscopy (SIM), liquid metal ion sources, focused gallium probes, secondary ion mass spectrometry (SIMS), high spatial resolution, imaging microanalysis, multiphoton ionization (MPI), multiphoton resonance ionization (MPRI), time of flight spectrometry, high mass resolution, atomic sputtering, laser ionization, post-ionization of sputtered atoms (PISA).

*Address for correspondence:
R. Levi-Setti, Enrico Fermi Institute
The University of Chicago, 5640 S. Ellis Ave
Chicago, IL 60637 Phone No. (312) 962-7827

Introduction

We have explored the feasibility of using laser non-resonant Post-Ionization of Sputtered Atoms (PISA), in conjunction with a Time of Flight (ToF) mass spectrometer, for the purpose of high lateral resolution imaging microanalysis in a Scanning Ion Microprobe (SIM).

As recently reviewed [Reuter, 1986], PISA techniques are emerging as practical and attractive alternatives to Secondary Ion Mass Spectrometry (SIMS). Among these, we regard non-resonant Multi-Photon Ionization (MPI) [Becker and Gillen, 1984, 1986], as the approach most likely to overcome the limitations which beset conventional SIMS imaging microanalysis methods. We qualify our advocacy of this approach, based on our experience with the University of Chicago-Hughes Research Laboratory Scanning Ion Microprobe (UC-HRL SIM) [Levi-Setti et al., 1985, 1986] and its RF-quadrupole-based SIMS system.

Notwithstanding the outstanding success of this instrument in imaging microanalysis (lateral resolution in the 20-90 nm range with a 2-40 pA, 40-60 keV Ga^+ probe), limitations have been encountered. Some of these are due to the trade-off between sensitivity and spatial resolution, others are intrinsic to the SIMS method, and others stem from the use of a quadrupole mass filter. In general, the ability to obtain detailed (high statistical accuracy) elemental maps is restricted by: i) The limited number of atoms in the microvolume probed in acceptable times. SIM optical columns based on the use of liquid metal ion sources (LMIS) are chromatic-aberration limited, because of the relatively large energy spread (5-10 eV) of LMIS. In such systems, the probe current density is independent of probe size, so that the probe current decreases with the square of the probe size. ii) The variability of the ion fraction, γ, of the sputtered atoms over a wide range (10^{-1} - 10^{-6}). In conjunction with i) above, this implies that only elements of low ionization potential or high electron affinity can be mapped with sufficient statistical accuracy to yield high resolution images. (The ion fraction is also sensitive to matrix effects.) iii) The limited transmission (η) of an RF quadrupole mass filter (10^{-1} - 10^{-4}) [Wittmaack, 1982]. The transmission is rapidly suppressed in the high mass range (>50 amu), and decreases almost exponentially, for large masses, with increasing mass resolution $M/\Delta M$. The useful range of the latter does not exceed ~ 300 for most commercial instruments. iv) A basic flaw is associated with all imaging SIMS systems which are tuned to transmit a selected ion species: the serial read-out of maps for different masses. This approach is inherently wasteful in terms of sample consumption, and the retrieved compositional information is

never truly contemporaneous: each elemental map refers to a different depth layer in the sample.

It should be noted that the shortcomings iii) associated with the use of quadrupole mass filters are greatly reduced by the use of magnetic sector, double-focusing mass spectrometers [Liebl, 1978]. The serial read-out problem iv) and to a great extent also the transmission and mass resolution limitations iii) can be eliminated with the use of ToF mass spectrometers [Niehuis et al., 1986].

Perhaps the most damaging limitation of SIMS microanalysis is ii), that caused by the intrinsic low ion yield of several important elements, e.g. N, P, Zn, Ag, Cu, Sn, Sb, Hg, in either positive or negative Ion-Induced Secondary Ions (ISI). Often, the limited dynamic sensitivity range in high resolution SIMS imaging (3 - 4 decades) prevents the useful detection of such elements. The PISA approach, for reasons well-summarized in the review by Reuter [1986], may offer the feasibility of high resolution localization of such problem species. This paper proposes a practical scheme for the utilization of non-resonant PISA (MPI) for high resolution imaging microanalysis, with calculations to support the feasibility of such a scheme.

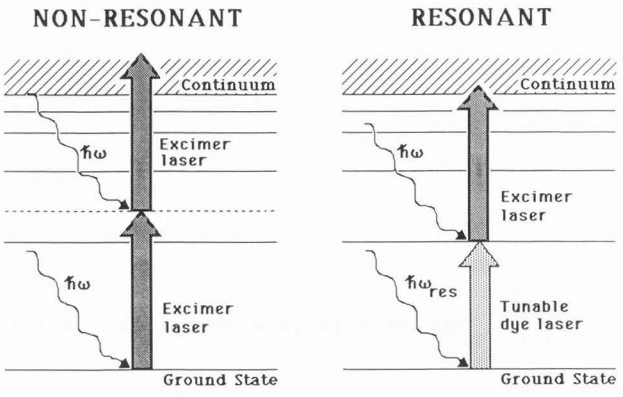

Fig. 1. Schematic energy diagram of two avenues of atomic multiphoton ionization.

Multi Photon Resonant Ionization and Non-Resonant Multi Photon Ionization

Two methods for laser-induced PISA have been demonstrated which can, in most cases, saturate the transitions from the ground or excited state of sputtered atoms to the continuum. The energy diagrams for these processes are shown in Fig. 1. In the non- resonant approach, Multi Photon Ionization (MPI) is achieved [Morellec et al., 1982], through the piling up of two or more photons until the ionization threshold is exceeded. The intermediate states are not eigenstates of the atom, but are regarded as "virtual" states. Conversely, Multi Photon Resonance Ionization (MPRI) is achieved through a resonant transition to an excited atomic state. [see e.g., Hurst et al., 1979 for a review]. One or more additional photons may be needed for a final transition to the continuum. In the application of MPI to microanalysis [Becker and Gillen, 1984, 1986], laser pulses from a high power excimer laser provide the photon field (10-100 mJ/pulse) required to saturate the ionization of the sputtered atoms. In the applications of MPRI [Hurst et al., 1979], [Parks et al., 1983], [Pellin et al., 1984], [Kimock et al., 1984], [Donohue et al., 1985], a tunable dye laser provides the photons for both the resonant transition as well as for the next, not necessarily resonant, transition to the continuum. Due to the large resonant cross sections, saturation is achieved with less laser energy (5-10 mJ/pulse).

Relevant for MPI are the elemental ionization potentials, plotted in Fig. 2. Indicated in the margin of this plot are the energies of one and two photons (6.4 and 12.8 eV) from an ArF excimer laser (193 nm). Two-photon absorption is sufficient to ionize most elements of interest to microanalysis of solids. Note that the important elements H, N, O, F cannot be

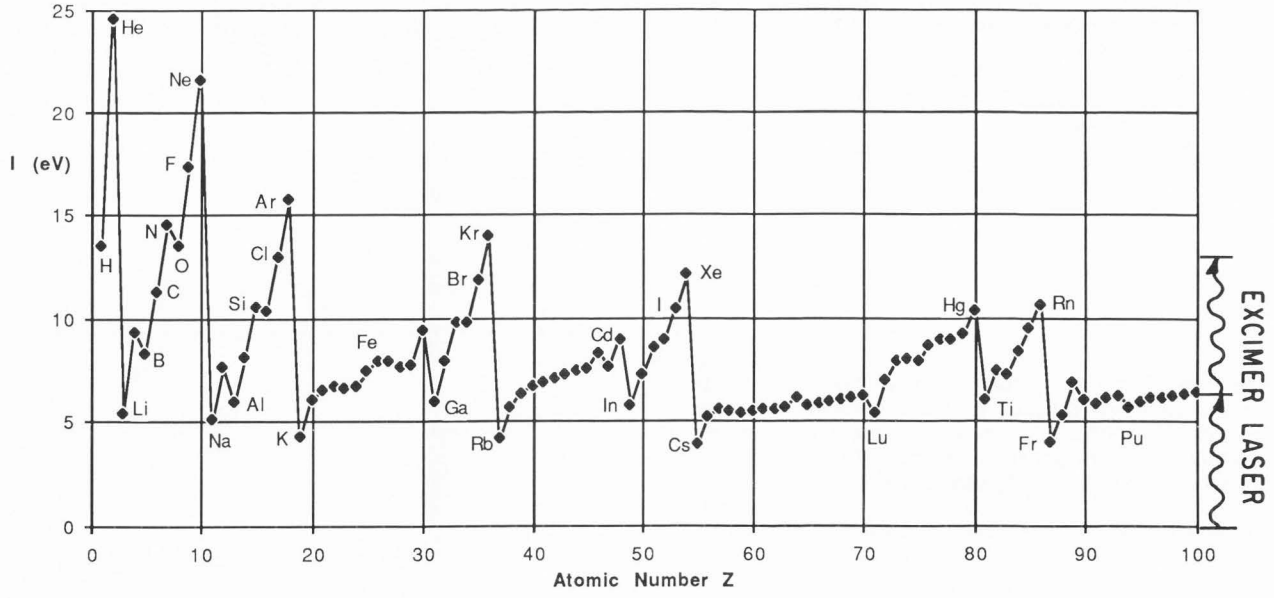

Fig. 2. Ionization potentials of the elements as a function of Z. The range of energies covered by two-photon non-resonant ionizaton (6.4 eV photons) is indicated in the right margin.

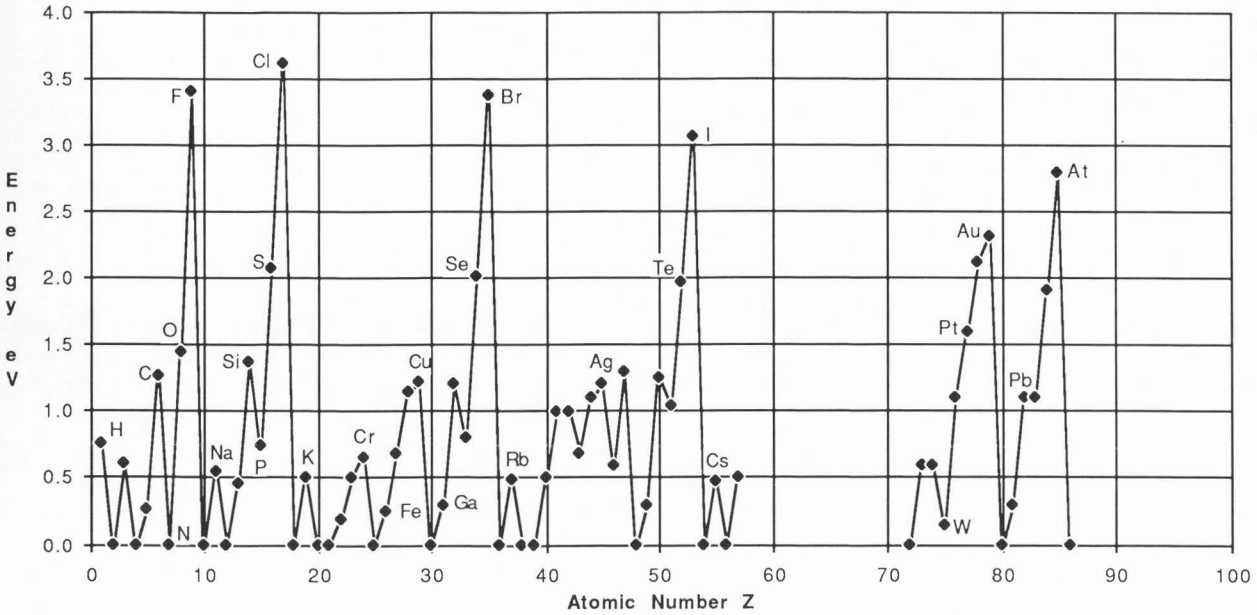

Fig. 3. Electron affinities of the elements as a function of Z.

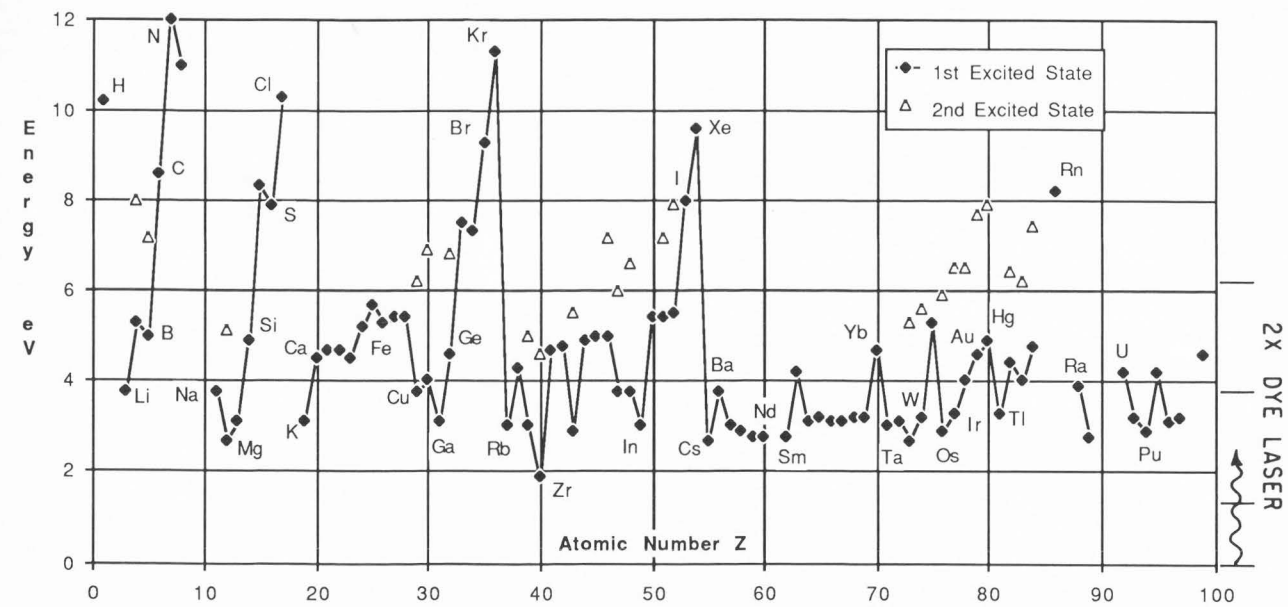

Fig. 4. First and second excited electronic states of the elements, as a function of Z. The typical energy range covered by photons from a tunable dye laser is indicated in the margin.

ionized with only two 6.4 eV photons. For completeness, we also plot in Fig. 3 the electron affinities of the elements. As is well known, due to their large electron affinity, H, O and F (and many other electronegative elements) exhibit large negative ISI yields. It is questionable whether PISA (MPI) is a worthwhile technique for such species.

Relevant for MPRI, Fig. 4 is a plot of the first and second excitation energies of the elements. Indicated in the margin is the energy range accessible with one photon from a tunable dye laser (Lambda Physik Dye Laser System (FL 2002)) and that reached with a frequency doubler (2x). The mass and energy state selectivity of resonant ionization effectively eliminates the need for mass spectroscopy, making MPRI an important tool for some applications. From the standpoint of quantification, although matrix and surface effects are expected to be greatly reduced relative to ISI emission, the method is still dependent on the particular state population of the sputtered atoms [Pellin et al., 1984].

We have carefully considered the relative merits of MPI vs. MPRI concerning their possible use for high resolution imaging microanalysis. In view of the discussion above on the shortcomings of conventional SIMS, we feel that the mass selectivity of MPRI is objectionable, as in the case for RF quadrupoles and magnetic spectrometers, because it leads to a serial read-out of mass information. Principally for this reason, we prefer to restrict our treatment here to the prospects

of PISA (MPI) coupled with ToF mass spectrometry and parallel read-out of mass-resolved images. Furthermore, it is expected that the independence of MPI from the state population (at saturation) may reduce matrix and surface effects, facilitating quantification. [Reuter, 1986].

Proposed PISA (MPI) high resolution scanning ion microprobe: Instrumental considerations

The realization of a useful high resolution PISA scanning ion microprobe hinges on the availability of: i) a pulsed, finely focused ion probe of high purity and sufficient intensity to compensate for the loss in sputtering power caused by the low duty cycle of the system; ii) a high power UV laser system of sufficient repetition rate to permit the acquisition of detailed images (> 256 x 256 pixels) in acceptable times; iii) an optimized scheme for the interaction of the laser beam with the cloud of sputtered neutral atoms; iv) a high mass resolution, high transmission ToF mass spectrometer; v) a data retrieval system capable of handling a very large amount of digitized information in real time.

Fig. 5 shows an exploded view of the MPI-PISA microprobe we propose. Its components will be discussed in relation to the above points.

Ion Probe

We believe that a LMIS-based optical column may form an adequate probe for PISA (MPI). As will be shown, even the low probe currents (~ 1 pA) at the limiting probe size so far obtained (~ 20 nm) [Levi-Setti et al., 1985, 1986] are sufficient for useful PISA (MPI). Furthermore, at a spot size of 100 nm, 40 pA of 40 keV Ga^+ ions are available in, for example, the UC-HRL SIM. Larger current densities have been obtained [Kurihara, 1985] with a slightly different optical design, yielding 1 nA at 60 keV in a 55 nm probe. Probes of higher energy are expected to yield even higher current densities. This can be seen as follows. In a LMIS optical column, the final spot size is dominated by chromatic aberration, due to the relatively large (5-10 eV) energy spread of the LMIS. The chromatic aberration probe diameter is

$$d_c = C\alpha \cdot \Delta E/E, \qquad (1)$$

where C is the coefficient of chromatic aberration of the lens system, α the probe semiangle, E the probe energy and ΔE the FWHM of the ion energy spectrum. Because the probe current density is given by:

$$J_p = \frac{4I_p}{\pi d_c^2} = 4\left(\frac{\alpha}{d_c}\right)^2 \frac{dI}{d\Omega}, \qquad (2)$$

where $dI/d\Omega$ is the angular intensity, for such a chromatically limited system we have:

$$J_p = 4\,\frac{dI/d\Omega}{\Delta E^2} \cdot \left(\frac{E}{C}\right)^2, \qquad (3)$$

which shows that J_p is proportional to the square of the probe energy. For this reason, among others, we are considering for the PISA microprobe, probe energies variable over a wide

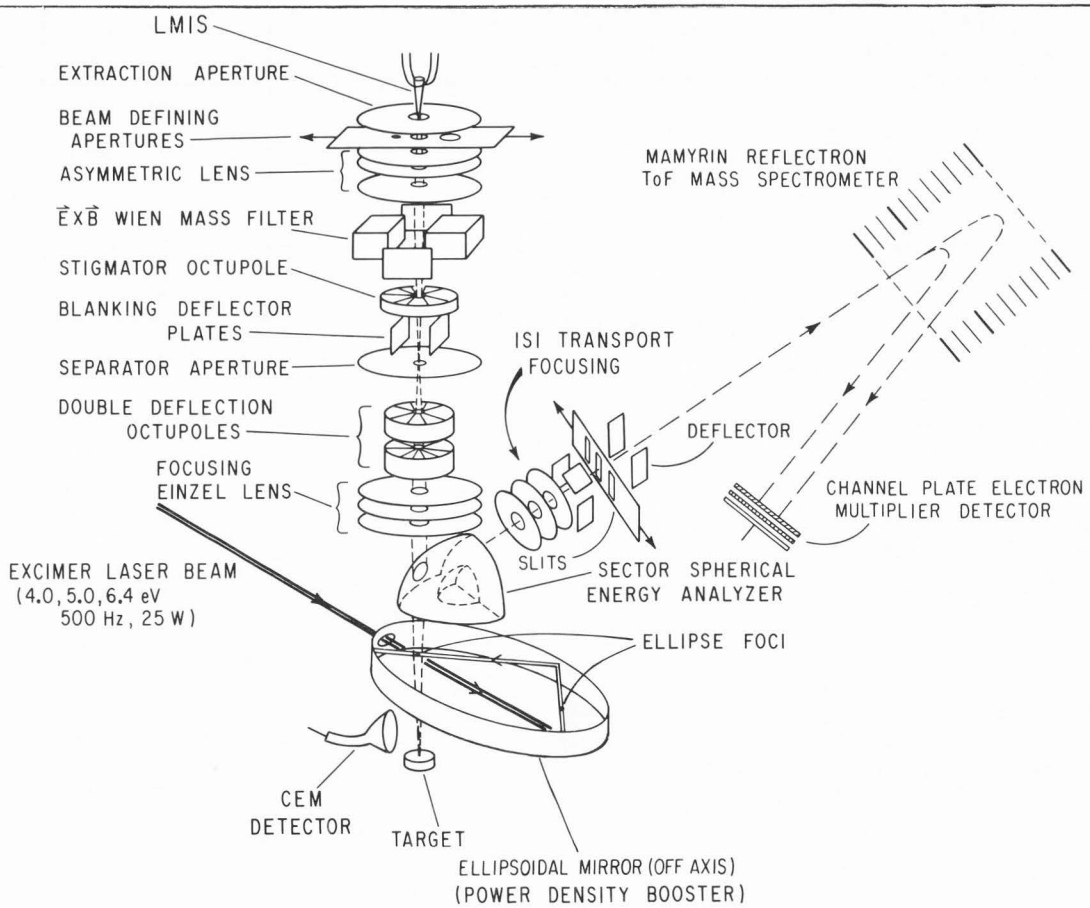

Fig. 5. Conceptual schematics of proposed high-resolution SIM based on laser-induced non-resonant post-ionization of sputtered atoms.

interval, e.g., 40-120 keV. It should be noted, though, that at high primary energies cascade mixing will reduce the depth resolution to a few hundred Å [Anderson, 1979].

A probe of high elemental purity will be required to fully exploit the proposed instrument's sensitivity. A Wien filter [Liebl, 1978, 1984], shown in Fig. 1, will produce this pure beam. It will also be necessary to blank the primary beam, to obtain probe pulses of length 0.1 - 10 μs. The pulse rise time will not be critical because the timing pulse for ToF spectrometry will be provided by the laser. An optical column which incorporates the above features is available ("NanoFab 150", Microbeam, Inc.) [Parker et al., 1986].

Laser system

A 500 Hz ArF (193 nm, 6.4 eV) UV excimer laser is presently manufactured (Lambda Physik model EMG 204 MSC). The laser pulses carry 200 mJ and have a 20 ns duration. A 1000 Hz laser of similar characteristics may also become available. At 500 Hz, with one pulse/pixel, a 500 x 500 pixel raster will be covered in 500 seconds. This is still an acceptable image acquisition time. With ion beam pulses of 1 μs duration, the duty cycle is 5×10^{-4}.

Post-ionization region

The optimization of the overlap region between the photon field and the cloud of sputtered atoms will be treated in detail in the next section. To increase the photon power density in the interaction region, we envisage the use of an off-axis ellipsoidal mirror, so that each laser pulse may interact several times with the neutral cloud. In the calculations to follow, we will assume a fivefold increase in power density (Booster factor B) due to this device.

Time of flight spectrometer

Fig. 5 shows a sector spherical electrostatic energy analyzer, which functions primarily as a collector-extractor of the ions from the interaction region. The accelerated ions will be analyzed by a "reflectron" ToF mass spectrometer [Mamyrin et al., 1973]. An appropriate alternative would be a Poschenrieder ToF spectrometer [Poschenrieder, 1972]. Both types of spectrometers have been used successfully in similar applications [Steffens et al., 1985], [Becker and Gillen, 1984], [Niehuis et al, 1986]. The reflectron type analyzer is characterized by isochronous energy focusing to first and second order. Very high mass resolution ($M/\Delta M > 10{,}000$) and high transmission (>10%) have been demonstrated [Niehuis et al., 1986]. In order to resolve molecular interferences, in most cases a mass resolution < 3000 is adequate. It is believed possible to attain a 50% ToF spectrometer transmission in these conditions. Including the energy analyzer transmission (estimated at ~20%), the overall transmission of the PISA ions should not be less than ~10%, compared to ~ 0.3% for the UC-HRL microprobe.

By appropriately adjusting the reflectron's potentials [Becker and Gillen, 1984] , it is possible to discriminate sputtered ions from post-ionized atoms.

Data retrieval

Methods for the acquisition of signals from a ToF spectrometer, through the use of a wide-band transient digitizer, have been detailed in the references given. In principle, one would like to acquire the entire mass spectrum for each laser pulse, corresponding to each setting of the probe. In practice, depending on the size of the computing facilities available, the parallel read-out of elemental maps will be limited to a few species of interest through routing of the signals appearing at preselected mass channels.

We collect in Table 1 the operating parameters of the proposed MPI-PISA scanning ion microprobe, with reference to Fig. 5.

TABLE 1
Operating Parameters of Proposed High-Resolution Scanning Ion Microprobe (Non-Resonant Two-Photon Ionization)

Ion source	LMIS with **ExB** mass filters
Ion Probe Voltage	40-120 kV
Ion Probe Current	1-100 pA
Lateral Resolution	15-150 nm
Probe Ion Pulse Length	0.1-10 μs
Photon Energy	6.4 eV (ArF)
Excimer Laser Energy	200 mJ/pulse
Laser Pulse Length	20 ns
Laser Repetition Rate	500 Hz
TOF Mass Resolution $M/\Delta M$	100-3000
Mass Range	1-5000 amu
Image Accumulation Time (512 x 512 pixels)	~500 sec.

TABLE 2
Optimization of Ion Yield ($Y_{2\omega}{}^{+}$) from Non-Resonant Two-Photon Ionization of Ion-Probe Sputtered Atoms

INPUT PARAMETERS:

- Probe current (I_P)
- Mass of sputtered atom (M_2)
- Surface binding energy (sublimation energy) of sputtered atom (E_b)
- Sputtering yield (S)
- Energy distribution of sputtered atoms $N_O(E)$
- Laser pulse power (P_L)
- Laser power flux (F_L)
- Laser pulse length (T_L)
- Multiphoton ionization rate (W)
- Laser power density booster factor (B)
- Energy analyzer & TOF transmission (η)
- N–photon ionization cross section (σ_N)

VARIABLES:

- Probe pulse length (T_P)
- Laser beam radius (r_L)

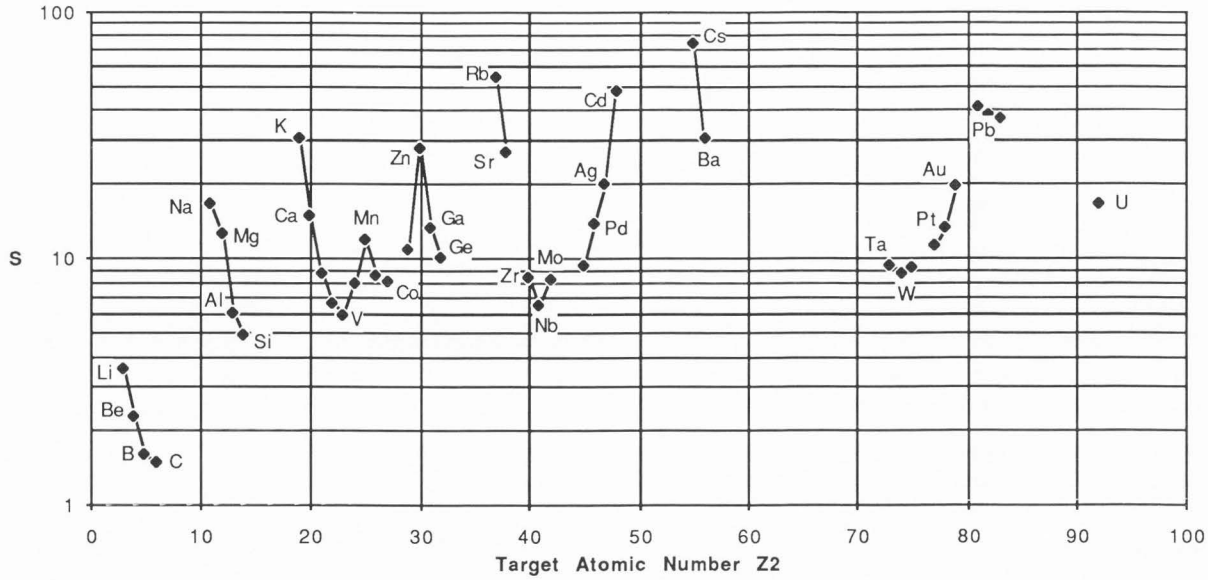

Fig. 6. Sputtering yields S of the elements, calculated from Sigmund [1969], as a function of target atomic number Z_2, for 40 keV Ga^+ incident ions.

Calculation of the yields of post-ionized sputtered atoms

In this calculation, which follows several of the arguments developed by Kimock et al. [1984], certain simplifying assumptions have been made which allow the derivation of an analytical form for the prediction of the PISA intensity.

In order to maximize the yield $Y_{2\omega}{}^+$ of two-photon ionized (MPI) atoms, it is critical to optimize the spatial overlap between the photon field and the cloud of sputtered neutrals. The variables of interest are the size of the laser beam (defined by a radius r_L for a cylindrical beam), and the pulse length T_p of the primary ion beam. A large number of input parameters is involved, using the nomenclature defined in Table 2.

Sputtering yields

Using the formalism given by Sigmund [1969], we have calculated the sputtering yields of 40 keV Ga^+ ions incident on pure elements. The factors $\alpha(M_2/M_1)$ and $S_n(\varepsilon)$ were obtained from Fig. 13 and Table I of Sigmund [1969]. The binding energy E_b was approximated by the latent heat of sublimation [Smithells, 1962]. These yields are shown in Fig. 6.

We realize that these calculated sputtering yields may not always correspond to measured yields, particularly due to uncertainties in the surface binding energy of compound targets. However, for the specific choice we made of 40 keV Ga^+ incident projectiles, they provide an otherwise unavailable systematic input to our calculations. S varies over almost two orders of magnitude. These variations, intrinsic to the sputtering process, unavoidably contribute (as a lower limit) to the range of both secondary ion and post-ionized atom yields from ion bombardment of solids.

Spatial distribution of the sputtered neutrals

We will assume [Thompson, 1968] that the energy distribution of the secondary neutrals from a polycrystalline surface can be written, after integration over the angular distribution, as

$$\frac{dN_0}{dE} = \frac{2SEE_b}{(E+E_b)^3} \quad , \tag{4}$$

where S is the sputtering yield and E_b is the surface binding energy. For a primary ion pulse of width dt and constant amplitude I_p occurring at time t = 0, the radial distribution of sputtered particles at a later time t can be found by substituting $E = {}^1/_2\, M_2({}^r/_t)^2$ and $dE = M_2 r\, dr/t^2$ into equation (4):

$$\frac{dN_0}{dr} = \frac{4I_pSdt}{r}\left(\frac{r}{tv_b}\right)^4\left(\frac{r^2}{t^2v_b^2}+1\right)^{-3} \quad , \tag{5}$$

where $v_b = (2E_b/M_2)^{1/2}$ and t is the time elapsed since emission. For a primary ion pulse of width T_p, (5) can be integrated with respect to t to obtain the particle radial distribution at time T_p:

$$\frac{dN_0}{dr} = \left(\frac{I_pST_p}{2v_b}\right)\left[\tan^{-1}\chi + \frac{\chi^2-1}{(\chi^2+1)^2}\right] \quad , \tag{6}$$

where $\chi = v_bT_p/r$ is a dimensionless quantity.

A quantity of practical interest is the fraction of sputtered neutrals inside a hemisphere of radius r_L for fixed T_p (see Fig. 7):

$$F[x(r_L)] = \frac{1}{(I_pST_p)}\int_0^{r_L}\left(\frac{dN_0}{dr}\right)dr = \frac{1}{2}\left(\frac{1}{x^2+1}+\frac{1}{x}\tan^{-1}x\right) \quad , \tag{7}$$

where $x = v_bT_p/r_L$.

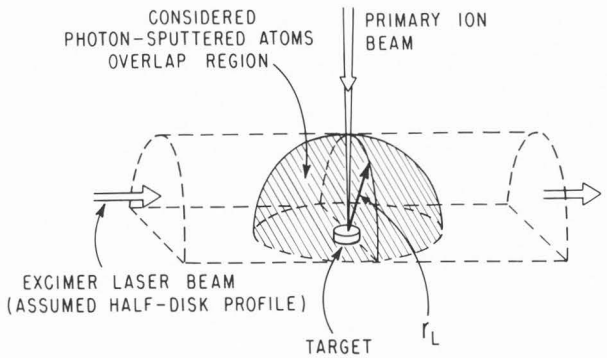

Fig. 7. The geometry adopted in the calculation of yields from two-photon non-resonant ionization of sputtered atoms.

Another quantity of interest is the relative number of neutrals inside a hemisphere of fixed radius r_L as a function of ion pulse-width T_p:

$$R[x(T_p)] = \frac{I_p T_p S F(x)}{\lim_{T_p \to \infty} [I_p T_p S F(x)]} \qquad (8)$$

$$= \frac{2}{\pi}\left(\frac{x}{x^2+1} + \tan^{-1} x\right) .$$

Plots of F(x) and R(x) are shown in Fig. 8, as a function of x. Similar results for a specific sputtered atom (In) were reported by Kimock et al. [1984]. Our results, in terms of the reduced parameter x, extend the scope of the calculation to any atomic species. It is interesting to note (dashed line in Fig. 8) that for $T_p > r_L/v_b$ (i.e. $x > 1$), F(x) approaches $(4/\pi)(1/x)$, and the number of particles $N_0(r_L)$ contained in a hemisphere of radius r_L is

$$N_0(r_L) = I_p S \frac{\pi}{4} \frac{r_L}{v_b} , \qquad (9)$$

independent of T_p.

Yield of two-photon ionized atoms in non-resonant PISA

It has been established [Morellec et al., 1982] that an ionization rate W can be defined whose dependence on the laser power flux F_L (W/cm^2) is

$$W = \sigma_N F_L^N , \qquad (10)$$

where σ_N is the total generalized N-photon ionization cross-section. The two-photon ionization probability $\alpha_{2\omega}^+$ of an atom in a laser pulse of width T_L is therefore:

$$\alpha_{2\omega}^+ = 1 - \exp(-\sigma_2 F_L^2 T_L) . \qquad (11)$$

For an order of magnitude estimate such as we seek in this feasibility study, σ_2 is $\sim 10^{-11}$(cm^{4}W^{-2} s^{-1}) when F_L is measured in W/cm^2.

Assuming the position of the sputtered neutrals as "frozen" during the laser pulse duration (~ 20 ns), the two-photon ionization yield can be written as

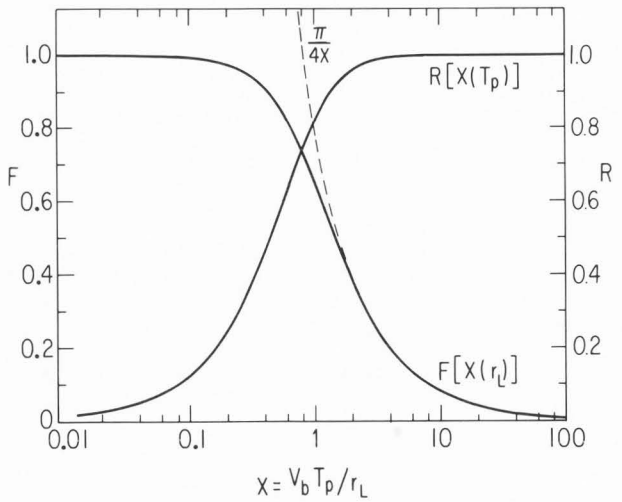

Fig. 8. $F[x(r_L)]$ is the fraction of sputtered neutrals within a hemisphere of radius r_L for fixed T_P. $R[x(T_P)]$ is the relative number of neutrals, as a function of T_P, within a hemisphere of fixed radius r_L. The dashed line is $\pi/4x$. See equations 7 through 9.

$$Y_{2\omega}^+ = \alpha_{2\omega}^+ \int_{V_L} \frac{dN_0}{dV} dV \qquad (12)$$

for a photon field-neutrals overlap volume V_L, where dN_0/dV is the density distribution of the neutrals.

We now approximate the overlap volume V_L by a hemisphere of radius r_L (Fig. 7), assuming a half-cylindrical laser beam. In so doing, we neglect a small fraction of neutrals intercepted by the laser beam outside of the hemisphere. The advantage of this approximation is that we can now express dN_0/dV in terms of dN_0/dr, previously calculated in eq. (6). Eq. (12) can be rewritten:

$$Y_{2\omega}^+ = \left[1 - \exp\left(-\frac{\sigma_2 P_L^2 T_L}{(1/2\,\pi r_L^2)^2}\right)\right] I_p S T_p F(x) \qquad (13)$$

We will discuss the optimization of r_L for the condition $T_p > r_L/v_b$, the range of practical interest. In this range, N_0 is independent of T_p.

$$Y_{2\omega}^+ = \left[1 - \exp\left(-\frac{\sigma_2 P_L^2 T_L}{(1/2\,\pi r_L^2)^2}\right)\right] I_p S \frac{\pi}{4} \frac{r_L}{v_b} \qquad (14)$$

$$= I_p S \frac{\pi}{4} \frac{\rho}{v_b} g(z) , \qquad (15)$$

where $$\rho = \left(\frac{\sigma_2 P_L^2 T_L}{(1/2\,\pi)^2}\right)^{1/4}$$

$$z = \frac{\rho^4}{r_L^4}$$

and $$g(z) = \frac{1 - \exp(-z)}{z^{1/4}}$$

The function g(z) reaches its maximum of 0.73 when z is 2.34, giving

$$Y^+_{2\omega max} = 0.73\, I_p \cdot S\, \frac{\pi}{4}\, \frac{1}{v_b} \left(\frac{\sigma_2 P_L^2 T_L}{(1/2\pi)^2} \right)^{1/4} \qquad (16)$$

$$\text{for } r_L = \left(\frac{\sigma_2 P_L^2 T_L}{2.34(1/2\pi)^2} \right)^{1/4}.$$

Substituting $\sigma_2 \approx 10^{-11}$ cm^{4}W^{-2}s^{-1}, we obtain the following estimate for the yield of two-photon PISA ions per laser pulse:

$$Y^+_{2\omega} = 2.1 \times 10^{-5}\, I_p \cdot S(T_L)^{1/4} \left(\frac{P_L M_2}{E_b} \right)^{1/2}, \qquad (17)$$

where I_p is in pA, T_L in ns, P_L in watts, M_2 in a.m.u., E_b in eV, and we have used the definition $v_b = (2E_b/M_2)^{1/2}$.

As an example, for $P_L = 10^7$ W, $T_L = 20$ ns, one finds $r_L \sim 0.4$ mm. In these conditions, the laser power density would be $\sim 4 \times 10^9$ W/cm^2, and $\alpha_{2\omega}{}^+ \sim 0.9$, comparable to the values reported by Becker and Gillen [1984].

The condition $T_p > r_L/v_b$ is easily achieved experimentally. For atomic masses of 1 amu and 300 amu, r_L/v_b is 22 ns and 390 ns, respectively (v_b is taken to be 5 eV). Because R(x) of eq. (8) saturates for $x > 4$, $4(r_L/v_b)$ is the practical upper limit for T_p.

If the laser pulse flux in the overlap region is increased by a factor of B (Booster factor) by multiple traversals through an ellipsoidal mirror system, the laser beam radius r_L sufficient to achieve two-photon PISA saturation will be larger by a factor of $B^{1/2}$ (see eq. 16). Correspondingly, yields from eq. (17) will be augmented by the same factor.

Predicted PISA yields of proposed scanning ion microprobe

Based on the use of an excimer laser delivering 200 mJ pulses of 6.4 eV photons at 500 Hz, and for B = 5, we have calculated from (17) the expected two-photon PISA yields for a 40 keV Ga^+ probe for all target elements for which E_b could be found. Expressed in number of created ions per second per pA of primary ion current, these yields are plotted in Fig. 9. The plot does not include values of $Y_{2\omega}{}^+$ for the alkali metals, for which the PISA approach offers no advantage over SIMS. The extent and periodicity of the variations of $Y_{2\omega}{}^+$ vs. Z, reflecting the atomic shell effects already present in S vs Z, are governed by variations in E_b, principally in the sputtering factor ($S \sim E_b^{-1}$). An additional $E_b^{-1/2}$ dependence arises from the photoionization process. The overall average increase of both S and $Y_{2\omega}{}^+$ vs. Z is caused by the mass dependence of S.

Although the amplitude of the $Y_{2\omega}{}^+$ vs. Z oscillations is reduced to ~ 1 - 2 orders of magnitude, versus 4 - 5 for the ion yields in SIMS, these intrinsic Z-effects must still be taken into account when relating observed PISA yields to relative elemental concentrations.

We collect in Table 3 the atomic accounting for a 512 sec scan with our present UC-HRL SIM/SIMS. This is to be compared with corresponding quantities estimated for the proposed PISA (MPI) SIM given in Table 4. The predicted numbers of detected counts is based on an average value of $Y_{2\omega}{}^+ \approx 10^4$ pA^{-1} sec^{-1} from Fig. 9.

TABLE 3
Atomic Accounting in Optimal SIMS Imaging

UC - HRL SIM/SIMS 512 sec Scan

PROBE SIZE	20 nm	100 nm
PROBE CURRENT	1.6 pA	40 pA
FIELD OF VIEW	20 x 20 μm^2	100 x 100 μm^2
AREA	4×10^{-6} cm^2	10^{-4} cm^2
SPUTTERED DEPTH (S = 10)	2.5 nm	2.5 nm
SPUTTERED VOL.	10^{-12} cm^3	2.5×10^{-11} cm^3
ATOMS IN VOL.	5×10^{10}	7.5×10^{11}
SIGNAL *	1.5×10^8	2.25×10^9

* For detected fraction of sputtered atoms $\eta\gamma = 3 \times 10^{-3}$, valid for elements of low ionization potential or high electron affinity.

TABLE 4
Atomic Accounting in PISA Imaging Optimized for Non-Resonant Two Photon Ionization

PISA (MPI) 512 sec Scan

PROBE SIZE	20 nm	100 nm
PROBE CURRENT	1.6 pA	40 pA
FIELD OF VIEW	20 x 20 μm^2	100 x 100 μm^2
AREA	4×10^{-6} cm^2	10^{-4} cm^2
DUTY CYCLE ($T_P = 0.5$ µs)	2.5×10^{-4}	2.5×10^{-4}
SPUTTERED DEPTH (S = 10)	0.64×10^{-3} nm	0.64×10^{-3} nm
SPUTTERED VOL.	2.6×10^{-16} cm	0.64×10^{-14} cm^3
ATOMS IN VOL.	1.3×10^7	3.2×10^8
DETECTED COUNTS * (AVERAGE)	9.2×10^5	2.3×10^7

* For detected fraction of photoionized atoms $\eta = 0.1$.

Discussion and Conclusions

Our calculations, summarized in Fig. 9 and Table 4, encouragingly predict both a feasible and practical utilization of the proposed high resolution SIM based on PISA (MPI). According to the estimates in Table 4, elemental maps (512 x 512 pixels per map, 512 sec scans) could be obtained with 4 counts/pixel at 20 nm probe size, 100 counts/pixel at 100 nm probe size. The yield loss due to the low duty cycle of the PISA system is partly compensated by increased detection

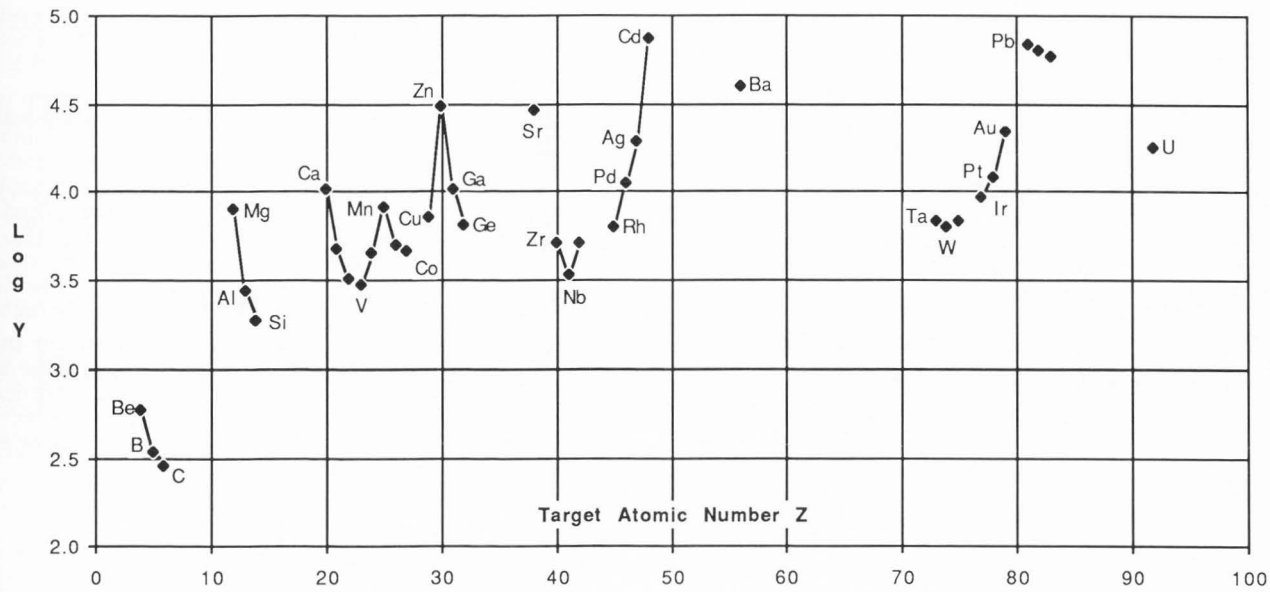

Fig. 9. Estimates of the ion yield s $Y_{2\omega}{}^{+}$ (ions $pA^{-1}s^{-1}$) of two-photon non-resonant ionization of atoms sputtered by a 40 keV Ga^{+} probe, as a function of target atomic number Z, for the operation parameters listed in Table 1.

efficiency. Though in comparison yields of sputtered ions from the UC-HRL SIM/SIMS (Table 3) are large, in practice high quality maps are obtained with overall statistics within the range predicted for the PISA (MPI) instrument. The higher SIMS yield is exploited to provide a larger number of pixels (1024 x 1024) and to permit shorter accumulation times. This advantage, however, is true only for a limited number of species with high ion fraction. For a large majority of species of low ion fraction, the advantages of SIMS are rapidly lost in favor of the PISA approach. In limiting cases, high resolution imaging is not possible by SIMS because of insufficient statistics; whereas, high quality maps could still be obtained with the proposed instrument.

We consider our yield estimates reliable to within an order of magnitude. A source of uncertainty is the two-photon ionization cross section σ_2, for which an average value of 10^{-11} $cm^4W^{-2}s^{-1}$ has been adopted from the data summarized by Morellec et al. [1982]. Although the range of σ_2 for different elements extends over ~4 orders of magnitude, σ_2 appears to the 1/4 power in the calculation of $Y_{2\omega}{}^{+}$.

The choice of laser beam geometry (a half disk cross section) for the analytical computation may not be realistic in practice. However, other geometries, carrying the required power density, should not affect our estimates significantly. In all cases, the necessary sub-millimeter-size laser beams used are within current technology. Critical is the setting of the laser beam to graze the target surface, to approximate the geometry of our calculation. The viability of increasing the laser power density (booster factor) by multiple reflections may be questioned. The reflections contribute, in our estimates above, only a factor of $\sqrt{5}$.

The choices for I_p in table 4 are very conservative. In fact, we demonstrate that viable maps can be obtained even at the pA level. Probe currents up to ~ 1 nA are possible which still preserve a probe size of 0.1 μm or better. This latitude ensures that our yield estimates can be attained and surpassed, even allowing for a large margin of error.

We believe high resolution imaging microanalysis by PISA (MPI) SIM is within reach of existing technology and represents an extremely worthwhile goal.

Acknowledgements

This work was supported by the NSF Materials Research Laboratory at the University of Chicago.

References

Anderson H H (1979). The depth resolution of sputter profiling. Appl. Phys. **18**, 131-140.

Becker C H, Gillen K T (1984). Surface analysis by non-resonant multi-photon ionization of desorbed or sputtered species. Anal. Chem. **56**, 1671-1674.

Becker C H, Gillen K T (1986). General postionization of sputtered and desorbed species by intense untuned radiation. Secondary Ion Mass Spectrometry, SIMS V. A. Benninghoven, R.J. Colton, D.S. Simons and H.W. Werner, (eds.) Springer-Verlag, NY. 85-89.

Donohue D L, Christie W H, Goeringer D E , McKown H S (1985). Ion microprobe mass spectrometry using sputtering atomization and resonance ionization. Anal. Chem. **57**, 1193-1197.

Hurst G S, Payne M G, Kramer S D, Young J P, (1979). Resonance ionization spectroscopy and one-atom detection. Rev. Mod. Phys. **51**, 767-819.

Kimock F M, Baxter J P, Pappas D L, Kobrin P H, Winograd N (1984). Solids analysis using energetic ion bombardment and multiphoton resonance ionization with time-of-flight detection. Anal. Chem. **5b**, 2782-2791.

Kurihara K (1985). A focused ion beam system for submicron lithography. J. Vac Sci. Technol. **133**, 41-44.

Levi-Setti R, Crow G, Wang Y L (1985). Progress in high resolution scanning ion microscopy and imaging microanalysis. Scanning Electron Microsc. 1985; II: 535-551.

Levi-Setti R, Crow G, Wang Y L (1986). Imaging SIMS at 20 nm lateral resolution: exploratory research applications. Secondary Ion Mass Spectrometry, SIMS V. A. Benninghoven, R.J. Colton, D.S. Simons and H.W. Werner, (eds.) Springer-Verlag, NY, 132-138.

Liebl H (1978). Limits of lateral resolution in ion probe microanalysis. Adv. in Mass Spect. **7A**, 751-757.

Liebl H (1984). High-resolution scanning ion microscopy and secondary-ion mass spectrometry: problems and solutions. Scanning Electron Microsc. 1984; II: 519-528.

Mamyrin B A, Karataev V I, Shmikk D V, Zagulin V A (1973). The mass-reflectron, a new nonmagnetic time-of-flight mass spectrometer with high resolution. Sov. Phys. JETP **37**, 45-48.

Morellec J, Normand D, Petite G (1982). Non-resonant multiphoton ionization of atoms. Adv. At. Mol. Phys. **18**, 97-164.

Niehuis E, Heller T, Feld H, Benninghoven A (1986). High resolution ToF secondary ion mass spectrometer. SIMS V. A. Benninghoven, R.J. Colton, D.S. Simons and H.W. Werner, (eds.) Springer-Verlag, NY, 188-190.

Parker N W, Robinson W P, Snyder, J M (1986): The NanoFab-150 -- A versatile new focused-ion-beam system. SPIE **632-09**, 76-84.

Parks J E, Schmitt H W, Hurst G S, Fairbank Jr. W M (1983). Sputter-initiated resonance ionization spectroscopy. Thin Solid Films **108**, 69-78.

Pellin M J, Young C E, Calaway W F, Gruen D M (1984). Trace surface analysis with pico-coulomb ion fluences: direct detection of multiphoton ionized iron atoms from iron-doped silicon targets. Surface Science **144**, 619-637.

Poschenrieder W P (1972). Multiple-focusing time-of-flight mass spectrometers Part II: ToFMS with equal energy acceleration. Int. J. Mass Spectrom. Ion Phys. **2**, 357-373.

Reuter W (1986). Post-ionization of sputtered particles. Secondary Ion Mass Spectrometry, SIMS V. A. Benninghoven, R.H. Colton, D.S. Simons and H. W. Werner, (eds.) Springer-Verlag, NY, 94-102.

Sigmund P (1969). Theory of sputtering I. Sputtering yields of amorphous and polycrystalline targets. Phys. Rev. **184**, 383-416.

Smithells C J (ed) (1962). Metals Reference Book II, 3d. ed. Butterworth & Co. Ltd., Washington, D.C., 618-619

Steffens P, Niehuis E, Friese T, Greifendorf D, Benninghoven A (1985). A time-of flight mass spectrometer for static SIMS applications. J.Vac. Sci Technol. **A3**, 1322 - 1323.

Thompson M W (1968). II: The energy spectrum of ejected atoms during the high energy sputtering of gold. Phil Mag. **18**, 377-414.

Wittmaack K (1982). Design and performance of quadrupole-based SIMS instruments: a critical review. Vacuum **32**, 65-89.

Discussion with Reviewers

W. Reuter: The authors are overly pessimistic in the reliability of the calculation of S. Using the formalism of Atomic Data Tables 31, I-80 (1984), which is a modified version of Sigmund, we find for metals and alloys agreement of about ± 30% using the admittedly questionable approach of atomic concentration averaging of E_b.

Authors: We appreciate your useful comment.

W. Reuter: The entire treatment in the paper is directed towards absolute intensities, the major concern in the work direction of the authors. Missing is any reference to the excellent capabilities of this technique primarily with standards to obtain relative atomic abundance data. It should be pointed out, that if $Y_{2\omega}{}^{+}{}_{A}/\ Y_{2\omega}{}^{+}{}_{B}$ in equations 16 and 17 is formed, S drops out. Then the only quantities which modify the relative concentration in the post ionized volume are differences in the elemental velocities (which one can calculate easily) and the respective radial density distribution assuming $\alpha_{2\omega}$ to be constant.

Data obtained by Becker indicate that the product $\alpha_{2\omega}{}^{+}\ \ {}^{dN_o}/_{dr}$ may not vary more than a factor of two. The calibration by the use of external composite standard, may reduce the accuracy of composited analysis to ± 10%.

Authors: Our primary concern here has been with an order of magnitude estimate of the expected ion yields in the proposed PISA microprobe, in order to justify its construction. We are aware that the use of standards will improve the reliability of quantification, even in the PISA approach. A large amount of literature is available on the use of standards in SIMS. A useful review of this topic is given by Werner (1980).

D.M. Gruen: There is insufficient discussion of the use of an ellipsoidal mirror to conclude that a fivefold increase in laser power density can in fact be achieved. For example, laser beam shape must be rigorously maintained so as not to damage the target. How will this be accomplished?

C.H. Becker: The booster optics puts the sample in the laser beam. There would be undesirable interactions between the sample and the intense laser beam. The booster optics may not be practical because of the laser beam divergence and losses on reflection.

Authors: The above questions relate to the same issue. We believe that the optical properties of elliptical mirrors will help preserve beam focus irrespective of angular divergence. The ellipse foci are stigmatic conjugate points: the ellipse is the locus of the equation r + r' = const, which is precisely an expression of the stigmatic condition for the foci taken as object and image points. Because, in addition, the magnification is unity in this case, in principle the beam spot size should remain constant. Due to imperfections of the mirror surface, this may not be rigorously true. We computed a booster factor B of 5 based on the conservative estimate of 10% loss per reflection. We wish to point out, however, that the factor B would enter to

the 1/2 power in eq (17), so that even if no power density boost were achieved, this would not rule out the feasibility of the PISA microprobe.

H. Liebl: Parallel readout of several elements is also feasible with magnetic double-focusing mass spectrometers (e.g. Mattauch-Herzog type) without the drawback of the limited duty cycle. Why didn't you take this possibility into consideration?
Authors: A magnetic double-focusing mass spectrometer is also a possible method of obtaining parallel mass read-out. However, because the duty cycle is imposed by the pulsed laser beam, no advantage is seen in this alternative approach.

H. Liebl: With higher primary ion energy the depth resolution deteriorates. What will it be with 120 keV ions from a liquid metal ion source?
Authors: We are aware that the depth resolution decreases with higher primary ion energy [Anderson, 1979]. We chose to consider higher primary energies in order to reduce the chromatic aberration of the probe, increasing the spatial resolution.

H. Liebl: The energy analyzer transmission is estimated at 20%. This would mean that 20% of the ionized atoms pass the entrance slit to the mass spectrometer. How is this accomplished?
Authors: Assuming that the energy analyzer transmits ions emitted within an acceptance angle Θ and within an energy window 0 - E_{max}, and assuming a $\cos\Theta$ dependence for the emitted secondary neutral intensity, we derive the following expression for the sector spectrometer transmission T:

$$T = \sin^2\Theta \left(1 - \sqrt{\frac{E_b}{E_{max}}}\right)$$

For example, for $\Theta = 45°$, $E_{max} = 20$ eV, and $E_b = 5$eV, we find $T = 0.25$.

N. Winograd: A difficulty with the non-resonant ionization method is that the laser must be tightly focused and it becomes tricky to maximize the spatial overlap between the desorbed particles and the photon field. Although this point has been nicely covered in the paper, the effect of having to direct the laser above the surface is not considered. How closely above the target do the authors feel they can safely position the laser focus and how big an effect will this have on the assumed sensitivity limits?
Authors: Our calculations indicate that the optimal overlap between neutral cloud and photon field will generally require a laser beam focused to a spot size of area ~ 0.25 mm^2 grazing the sample surface. In practice, to avoid laser beam-sample interaction, the laser beam will have to be placed at a certain distance d, above the surface. For a value of d equal to twice the radius of the optimal laser beam (0.8 mm), which we consider safe (Becker and Gillen, 1984), we estimate that our optimal yields of Fig. 9 will be reduced, to first order, by a factor $4d/\pi V_b T_p \approx 0.25$ ($V_b T_p \approx 10 r_L$).

D. M. Gruen: Why could one not use MPI and MPRI in combination so as to take advantage of the higher sensitivity of MPRI for elements present in low concentration?
Authors: Our study of feasibility does not rule out the use of MPRI, which could be implemented with the addition of a tunable dye laser and frequency doubler. This approach would naturally be advantageous in particular cases. Our consideration of MPI here shows that even the most unfavorable case, from the standpoint of photoionization cross-sections, leads to reasonable estimates of feasibility. The advantage of MPI rests with the ability to analyze the full mass spectrum simultaneously.

Reviewer VI: There will be a time delay associated with every pass of the reflected laser beam. How will this affect your estimates?
Authors: If the ellipsoidal mirror is small (< 10 cm principal axis), the laser pulse will be effectively lengthened while the booster factor will be reduced by a small amount. For example, if the mirror principal axis is 10 cm and the laser pulse is 20 ns long, and assuming a 10% loss per reflection, then the laser power density at the sample focus region will reach 90% of its peak value in 6 ns. After 20 ns, when the laser pulse ceases, the power density drops to 10% of its peak value in an additional 6 ns. By making the substitution $P_L \rightarrow P_L(t)B$ in eq. (14) (the time dependence of P_L is to remind us that the laser power changes in the interaction region), and by carefully summing the power density over the entire interaction, we find an effective booster factor of 3.81.

Additional Reference

Werner H W (1980). Quantitative Secondary Ion Mass Spectrometry: A Review. Surface and Interface Analysis **2**, 56-78.